Supporting Information for "Modeling the shape and velocity of magmatic intrusions, a new numerical approach"

S. Furst[1,3], F. Maccaferri[2], V. Pinel[1],

[1]Univ. Grenoble Alpes, Univ. Savoie Mont Blanc, CNRS, IRD, Univ. Gustave Eiffel, ISTerre, 38000 Grenoble, France

[2]Istituto Nazionale di Geofisica e Vulcanologia, Sezione di Napoli - Osservatorio Vesuviano, Via Diocleziano 328, 80124, Napoli, Italy

[3]GEOMAR Helmholtz Centre for Ocean Research Kiel, 24148 Kiel, Germany

Contents of this file

Introduction

In this supporting information, we develop the continuous equations for strain, gravitational and kinetic energy contributions (Text S1) that are stated in the main manuscript in sect. 2 and 5. The discretization of the continuity equation of fluid flow is also developed in Text S2. We provide for a flowchart illustrating the different steps of our numerical approach in Fig. S1. On Fig. S2 we display the numerical instabilities that rise for low fracture toughness (see sec. 4 and 5). We present in Tab. S1 the input parameters for the simulations performed in the Results section (sec. 4). We also provide complementary results on the fluid flow velocity (Fig. S3) and on the effect of input velocity on the dissipation energy contributions (Fig. S4). We supply our discussion section (sec. 5) with a figure of the kinetic energy contribution to the energy release (Fig. S5).

Text S1. Equations for strain, gravitational and kinetic energy contributions.

S1.1 Equations for strain energy contributions.

The **strain energy** W produced by the system includes the contribution from the elastic medium and from the compressible fluid. The work W_r performed against the elastic forces to open a fracture surface Σ by the amount equal to the Burger vector $\boldsymbol{b}$ is given by:

$$W_r(\Sigma) = -\frac{1}{2}\int_{\Sigma} b_i(\sigma^0_{ij} + \sigma^1_{ij})\upsilon_i d\Sigma \tag{S1}$$

with υ the unit normal to the surface Σ and σ^0, σ^1 the stress tensor acting on Σ before and after the displacement respectively. In 2D, the elastic energy due to a compressible fluid W_f undergoing a surface area change is defined by the work performed to compress

the fluid from the reference area A_0 to the area at the considered stage of propagation A:

$$W_f(A) = \int_{A_0}^{A} P(A)dA \tag{S2}$$

with $P(V)$ the pressure change acting on the volume of fluid.

S1.2 Equations for gravitational energy contributions.

The gravity potential G of the system also varies due to the work done to intrude a mass. The 2D gravitational contribution G_f due to the surficial mass $m = \rho_f A$ of the intrusion is given by:

$$G_f = -\int_V \rho_f g z A dA \tag{S3}$$

Maccaferri, Bonafede, and Rivalta (2011) have shown that the contribution of the gravitational energy due to the opening of the fracture is negligible.

S1.3 Equations for kinetic energy contributions.

In the crack problem, we consider **kinetic energy** of both the fluid and the rock. The kinetic energy of the fluid E_{cf} is due to the motion of all elementary fluid masses dm moving through the crack body $\mathcal{B}$ at a velocity u such as:

$$E_{cf} = \frac{1}{2}\int_{\mathcal{B}} u^2 dm \tag{S4}$$

The displacement of all elementary masses dM of rock body $\mathcal{C}$ at a velocity ω during the crack propagation also contributes to the kinetic energy of the system E_{cs} such as:

$$E_{cs} = \frac{1}{2}\int_{\mathcal{C}} \omega^2 dM \tag{S5}$$

The discrete equations of the strain and gravitational energy contributions are provided by Maccaferri et al. (2011) (eq. 14 and 15 for respectively W_r and W_f). We hereafter describe the discretized equations for the kinetic energy contributions.

S1.4 Discretized kinetic equations.

At a given propagation step k, the kinetic energy linked to the dislocation element i depends on the fluid mass m and on the vertical displacement of the fluid, such as :

$$E_{cf}^k = \sum_{i=1}^{N} \left[\frac{1}{2} \rho_m \cdot l \cdot \int_0^{h_i^k} \left(U_i^k(r) \right)^2 dr \right] \tag{S6}$$

with $\int_0^{h_i^k} \left(U_i^k(r) \right)^2 dr = \frac{6}{5} \cdot h_i^k \cdot < u_i^k >^2$ for a Poiseuille flow, we have:

$$E_{cf}^k = \frac{3}{5} \rho_m \cdot l \cdot \sum_{i=1}^{N} h_i^k < u_i^k >^2 \tag{S7}$$

with $< u_i^k >= \frac{f_i}{h_i^k}$.

Similarly to the fluid contribution, we can write the **kinetic energy of the rock**:

$$\lambda_i^k = \frac{1}{2} M_i^k \omega_i^2 \tag{S8}$$

where $M_i^k = \rho_r |h_i^k - h_i^{k-1}| \cdot l$ is the mass of rocks displaced by the opening or closing of the dislocation element i at the propagation step k. ω_i is the average velocity at which the mass M_i^k is displaced, and can be written as the displacement variation $|h_i^k - h_i^{k-1}|$, divided by the duration of the propagation step $\Delta t^k = l/v^k$. Therefore:

$$\omega_i = \frac{h_i^k - h_i^{k-1}}{l} v^k \tag{S9}$$

The total kinetic energy of the solid is defined by:

$$E_{cs}^k = \frac{1}{2} \rho_r \frac{(v^k)^2}{l} \sum_{i=1}^{N} |h_i^k - h_i^{k-1}|^3 \tag{S10}$$

Between two propagation steps, the **variations of kinetic energies** can be written as:

$$\begin{cases} \Delta E_{cf} &= E_{cf}^k - E_{cf}^{k-1} \\ \Delta E_{cs} &= E_{cs}^k - E_{cs}^{k-1} \end{cases} \tag{S11}$$

And it follows that the total contribution of kinetic energies ΔE_c (Fig. S3) is given by:

$$\Delta E_c = \Delta E_{cf} + \Delta E_{cs} \tag{S12}$$

Text S2. Discretizing continuity equation of incompressible fluid flow.

For an incompressible fluid flow, eq. 5 can be written as:

$$\frac{\partial h(s,t)}{\partial t} = -\frac{\partial f(s,t)}{\partial s} \tag{S13}$$

Integrating eq. S13 over time from t to $t + \Delta t$ and over the curvilinear abscissa from s to $s + ds$ provides the fluid flow at a dislocation element i between two propagation steps $k-1$ to k, such that:

$$\frac{h_i^k - h_i^{k-1}}{\Delta t} = -\frac{f_i^{top} - f_{i-1}^{top}}{l} \tag{S14}$$

where $l = ds$ being the dislocation length. It follows that,

$$f_i^{top} = -f_{i-1}^{top} - l \cdot \frac{h_i^k - h_i^{k-1}}{\Delta t} \tag{S15}$$

Introducing the volume variations associated with each dislocation element during Δt (eq. 14) leads to:

$$\begin{aligned} f_i^{top} &= -f_{i-1}^{top} - \tfrac{\Delta V_i}{\Delta t} \\ &= -\tfrac{1}{\Delta t}\Sigma_{j=1}^{i}\Delta V_j \end{aligned} \tag{S16}$$

References

Maccaferri, F., Bonafede, M., & Rivalta, E. (2011, November). A quantitative study of the mechanisms governing dike propagation, dike arrest and sill formation. *Journal of Volcanology and Geothermal Research*, *208*(1-2), 39–50. doi: 10.1016/j.jvolgeores.2011.09.001

Spence, D. A., & Turcotte, D. L. (1990). Buoyancy-driven magma fracture: A mechanism for ascent through the lithosphere and the emplacement of diamonds. *Journal of Geophysical Research*, *95*(B4), 5133. doi: 10.1029/JB095iB04p05133

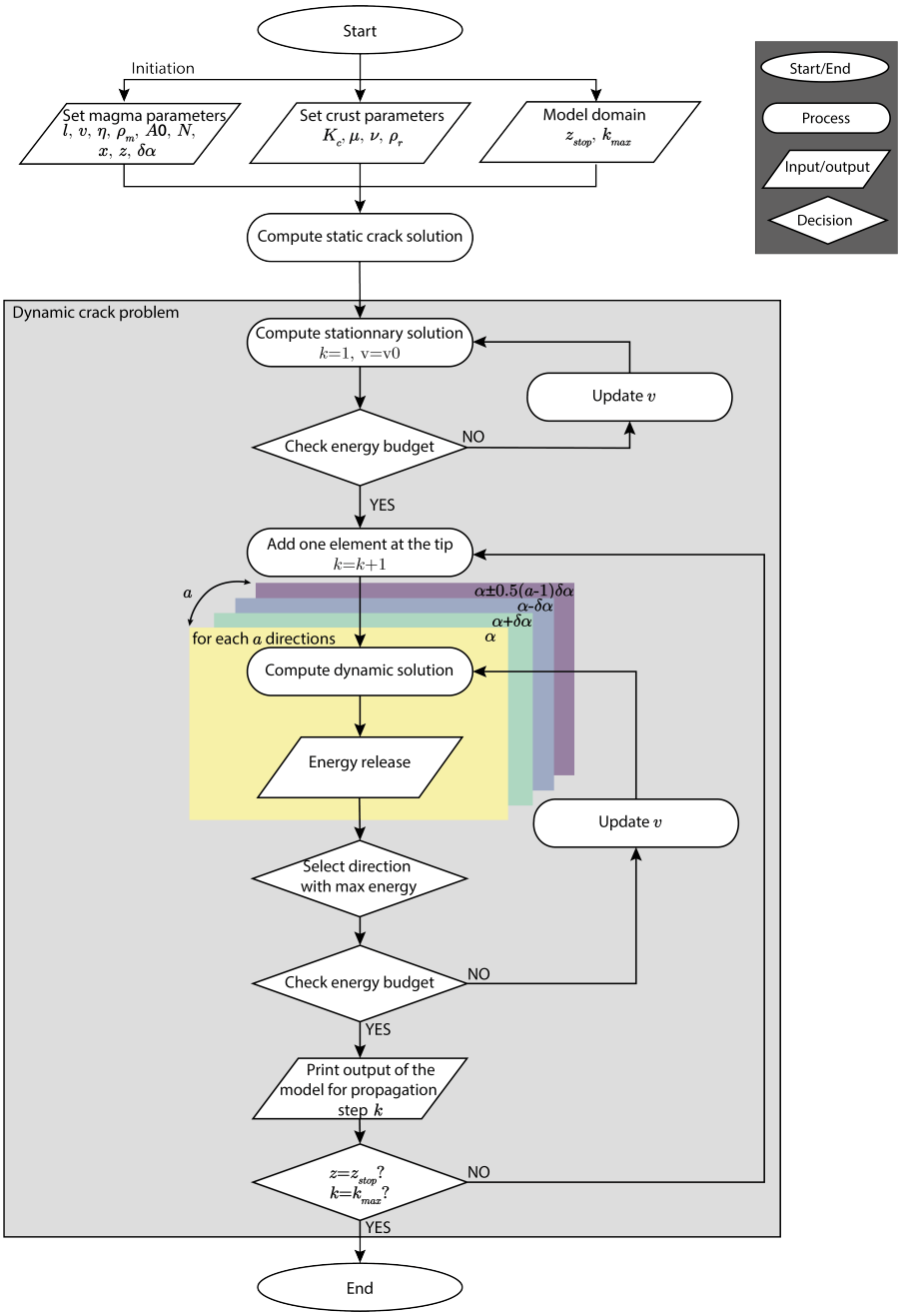

Figure S1. Flowchart of the numerical approach. Diagram representing the different steps of the numerical approach described in this study. The numerical approach stops either when the crack tip has reached a prescribed depth ($z = z_{stop}$), or when the number of propagation steps has reached a prescribed value ($k = k_{iter}$).

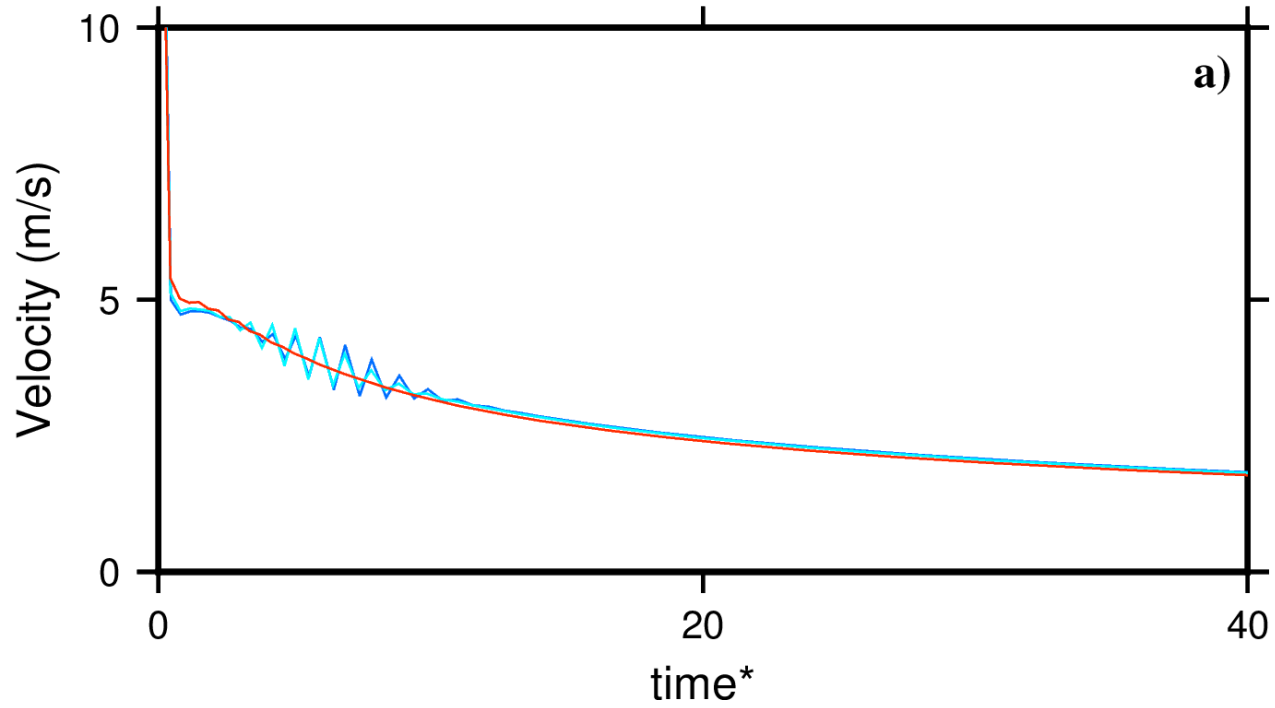

Figure S2. Numerical instabilities. Velocity of propagation as function of dimensionless time (eq. 4 from Spence & Turcotte, 1990) for simulations with identical parameters as in Fig. 2 and for low energy threshold: E_f= 5, 4.8, 4.6 MPa·m in red, cyan and blue respectively.

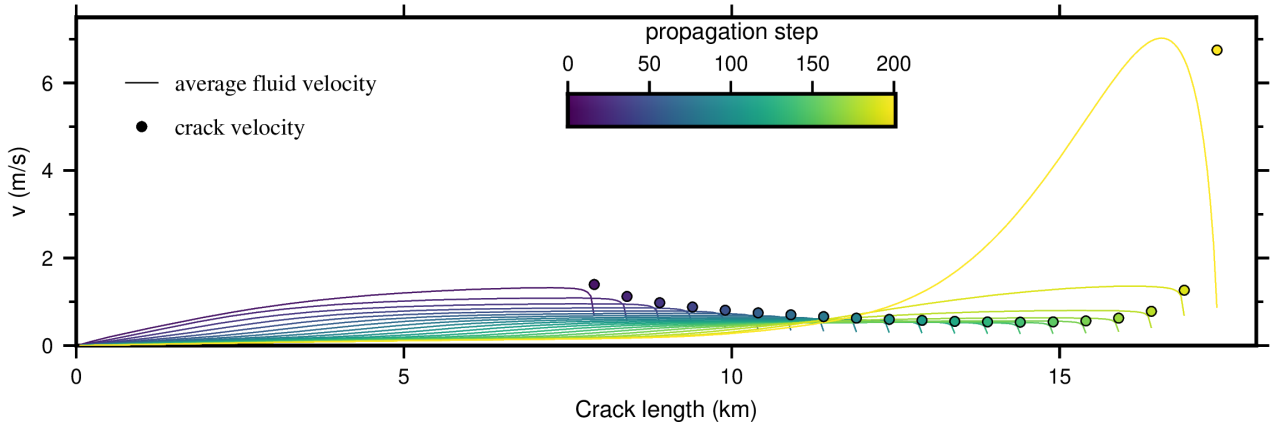

Figure S3. Fluid velocity. Comparison between the average Poiseuille fluid flow velocity estimated at the center of each dislocation element using eq. 18 (continuous lines) and the crack propagation velocity (colored circles) at different propagation steps for our reference case (first row of Tab. S1).

Table S1. Parameters for all the simulations performed in sec. 4.2 and 4.3: rigidity (μ), rock density (ρ_r), magma density (ρ_m), viscosity (η), compressibility (K), input velocity (v_0), depth (z), cross-sectional area (A_0), dislocation length (l), initial dyke length (L), fracture energy (E_f), fracture toughness (K_c) and mean velocity (v_{mean}). The red numbers indicate the range of parameters that were used in the simulations for the parametric analysis (sec. 4.3) compared with the reference case. K_c is deduced from eq. 6 and v_{mean} is the average dyke velocity excluding the initial phase of crack growth and the final acceleration due to the free surface (for 0.9< z^* <0.1).

μ (GPa)	ρ_r (kg/m^3)	ρ_m (kg/m^3)	η (Pa.s)	K (GPa)	v_i (m/s)	z (km)	A_0 (km^2)	l (km)	L (km)	E_f (MPa.m)	K_c (MPa.m$^{1/2}$)	v_{mean} (m/s)
20	3000	2700	100	20	[0.55-5.3315]	10	0.009	[0.025-0.1]	[6-7.4]	[4.6;24]	[495;1131]	[2.42;0.121]
20	3000	2700	[1;10000]	20	1.0	10	0.009	0.05	7.4	12	800	[124;0.01]
20	3000	2700	100	10	0.01	10	0.009	0.05	7.4	12	800	0.38
[5;30]	3000	2700	100	20	1.0	10	0.009	0.05	7.4	12	[400;980]	[3.75;0.94]
20	3000	2700	100	20	1.0	10	[0.005;0.012]	0.05	7.4	12	800	[0.11;2.44]
20	3000	2700	100	20	[0.8;1.9]	10	0.009	0.05	7.4	12	[800]	1.24

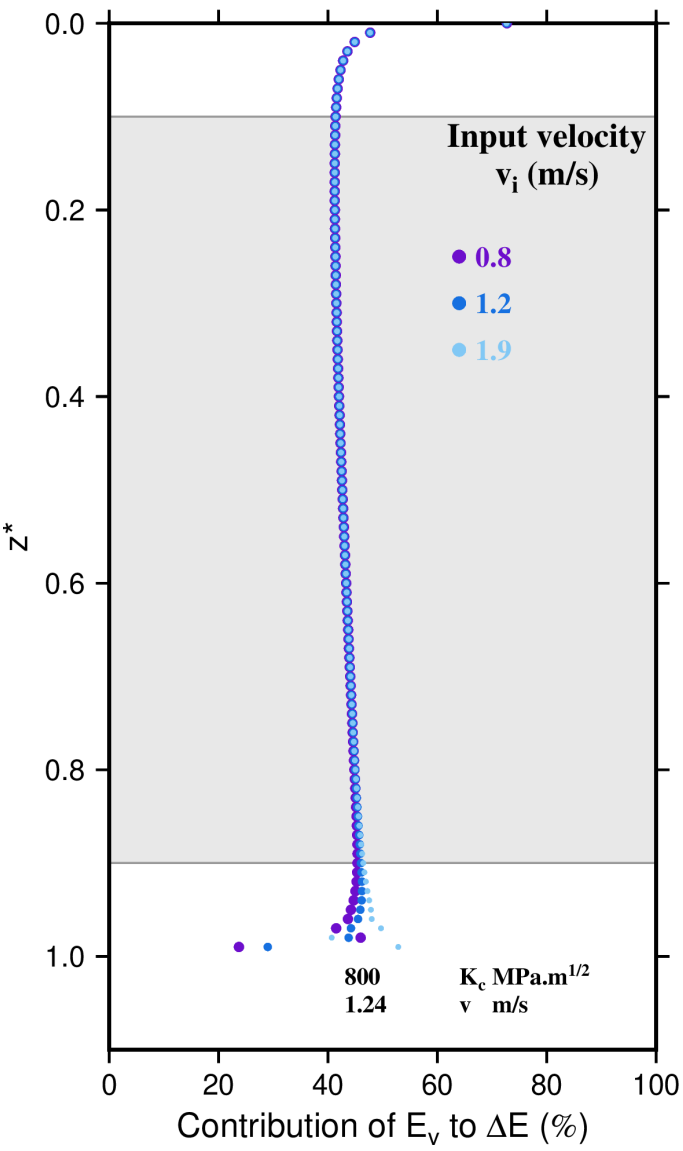

Figure S4. Effect of input velocity on energy contributions. Evolution of viscous dissipation contribution with respect to the total energy produced by the system, for magmatic intrusions ascending below the surface. z^* is the depth of the crack tip normalized by the initial depth for numerical simulations. Influence of the input velocity for a given set of parameters with fixed E_f=12 MPa.m (the sixth row in Tab. S1) corresponding to a K_c=800 MPa.m$^{1/2}$ as indicated at the bottom of the graph, along with the mean velocity of propagation estimated along the "constant part" of the propagation (defined by the grey domain).

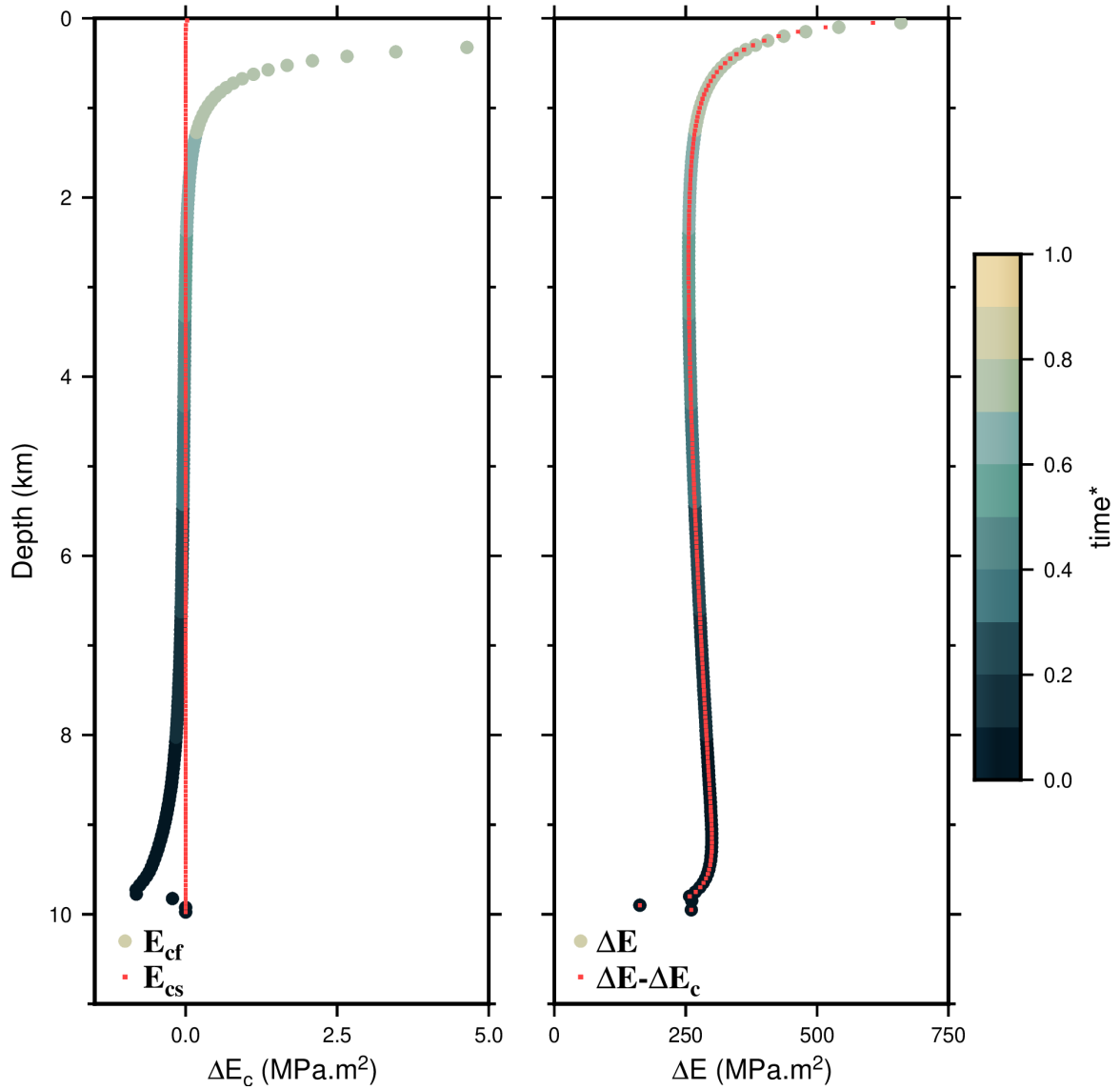

Figure S5. Magma and rock kinetic energy variations. a) Evolution of kinetic energy variations between two propagation steps due to the magma propagation ΔE_{cf} (colored circles) and to the opening and closure of the medium ΔE_{cs} (red dots) as defined by eq. S11. b) Evolution of the energy release ΔE (see sect. 2.4) between two propagation steps for the reference case (see Tab. S1, colored circles), and accounting for the kinectic energy variations ΔE_{cs} (eq. S12, red dots).